Downward influence of stratospheric final warming events in an idealized model

Lantao Sun[1] and Walter A. Robinson[2]

Received 10 November 2008; revised 11 December 2008; accepted 31 December 2008; published 12 February 2009.

[1] The stratospheric final warming is the final transition of the zonal winds from wintertime westerlies to summertime easterlies as solar heating of the high latitude stratosphere increases. Here the stratospheric influence on the tropospheric circulation during the stratospheric final warming events is investigated through ensemble model integrations of a simple dynamical core general circulation model. When the radiative equilibrium temperature in the stratosphere alone is gradually changed from a winter to a summer profile, the model generates realistic final warmings. As in the observations, the simulated final warmings occur at different "dates" in different realizations. Following previously published analyses of observed final warmings, we form a climatological springtime transition and compute composite anomalies centered on the final warmings. Simulations for both non-topographic and topographic cases show that starting five days before the final warming, the stratospheric zonal wind rapidly decelerates, in association with a strong upward Eliassen-Palm (EP) flux anomaly and EP flux convergence. Precursor events of wave driven zonal-wind deceleration occur, but at different times in simulations with and without topography. The composite zonal wind anomalies for final warmings with and without topography are compared with each other and with observations. In both cases, a statistically significant zonal wind anomaly extends downward to the surface, similarly to what is observed in the Northern Hemisphere (NH). These tropospheric zonal wind anomalies are stronger in the simulations with topography. Tropospheric geopotential height anomalies across the final warming also resemble NH observations. **Citation:** Sun, L., and W. A. Robinson (2009), Downward influence of stratospheric final warming events in an idealized model, *Geophys. Res. Lett.*, *36*, L03819, doi:10.1029/2008GL036624.

1. Introduction

[2] The stratospheric final warming is the final transition of the zonal winds from wintertime westerlies to summertime easterlies as solar heating of the high latitude stratosphere increases in springtime [*Andrews et al.*, 1987]. It differs from the mid-winter stratospheric sudden warming in that sudden warmings are controlled, to a large extent, by planetary waves originating in the troposphere, independently of background radiative forcing. While many studies have explored stratosphere-troposphere coupling during midwinter sudden warmings, only recently was it found that final warmings "may provide a strong organizing influence upon the large-scale circulation of both the stratosphere and troposphere during the period of spring onset" [*Black et al.*, 2006] (hereinafter referred to as BMR). The Northern Hemisphere (NH) observational analysis of BMR showed that a coherent pattern of significant zonal wind anomalies (defined as deviations from the climatological seasonal cycle) in the high latitudes of the stratosphere extends downward to the surface. In the Southern Hemisphere (SH), however, only marginally significant anomalies are observed in the troposphere [*Black and McDaniel*, 2007a]. Further analyses revealed that the downward influence during the NH final warmings could be divided into two stages: the stratospheric deceleration stage (day −10 to day 0, where day 0 is the onset date of the final warming), in which the tropospheric anomaly is due in part to a direct response to attendant redistributions of potential vorticity in the lower stratosphere, and the tropospheric deceleration (day 0 to day +10) stage, in which the stratosphere provides an indirect influence upon the high latitude troposphere by vertically trapping tropospheric planetary wave activity [*Black and McDaniel*, 2007b]. These observations suggest that the stratospheric final warming makes a significant contribution to the springtime transition in the lower atmosphere. The springtime transition is complex, however, and it is not possible, in observations, to separate unambiguously stratospheric influences from those governed by tropospheric processes alone. In a model, however, it is possible to induce a springtime transition - a final warming - only in the stratosphere, and the resulting tropospheric changes are then unquestionably attributable to the stratospheric final warming. In other words, only in a model is it possible to perform a clean test of the hypothesis, which is supported by strong, though circumstantial, observational evidence, that the stratospheric final warming is an important contributor to springtime changes in the circulation near Earth's surface. This is our motivation for the present study.

[3] Inspired by the work of *Held and Suarez* [1994], dynamical cores of atmospheric general circulation models (GCM) have been widely used to study, among other processes, the dynamical coupling of the stratosphere and troposphere [e.g., *Polvani and Kushner*, 2002; *Kushner and Polvani*, 2004; *Song and Robinson*, 2004; *Reichler et al.*, 2005]. In this letter, we explore the hypothesis that much of the observed tropospheric signal of the final warming is initialized from the stratosphere. Final warmings are simulated by imposing a transition in the radiative equilibrium temperature (T_{eq}) from winter to summer only in the stratosphere. Large ensembles of final warming events are run, from which composites are formed and compared with

[1]Department of Atmospheric Sciences, University of Illinois at Urbana-Champaign, Urbana, Illinois, USA.
[2]Division of Atmospheric Sciences, National Science Foundation, Arlington, Virginia, USA.

0094-8276/09/2008GL036624$05.00

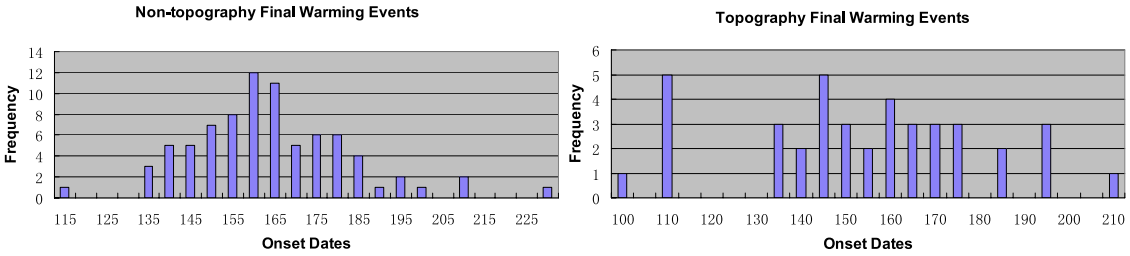

Figure 1. Histograms of the onset date for the (a) non-topography and (b) topography final warming events. The onset date is the number of days after the T_{eq} transition.

observations. The next section of this paper describes the model and the simulations; results are presented in part 3; and the final section presents a summary and discussion of these results.

2. Model and Simulation Methods

[4] A dynamical core GCM is used to simulate final warming events. This is a dry, primitive-equation, hydrostatic, spectral model derived from a 1990s version of the Geophysical Fluid Dynamics Laboratory atmospheric model. The same model was used by *Song and Robinson* [2004]; for the purposes of this study we have made some changes to the radiative equilibrium temperature (T_{eq}) field and to the Newtonian cooling rates. The model is run at rhomboidal 30 spherical harmonic truncation and 30 vertical levels, the same as used by *Scinocca and Haynes* [1998]. A small number of test cases are run at higher resolutions. In addition, we use a zonally symmetric version of our model, which is identical to the full model but excludes all planetary waves, for comparison with the full model.

[5] Temperatures are linearly relaxed to a zonally symmetric radiative equilibrium temperature (T_{eq}) field, which is computed from a radiative equilibrium zonal wind profile using the thermal wind relation (see auxiliary material[1]), and is similar to that used by *Scinocca and Haynes* [1998]. The winter and summer profiles of T_{eq} differ only in the stratosphere. The Newton cooling coefficient, α, is that used by *Holton and Mass* [1976],

$$\alpha(z) = \{1.5 + \tanh[(z - 35\,\mathrm{km}/7\,\mathrm{km})]\} \times 10^{-6}\mathrm{s}^{-1}, \qquad (1)$$

where z is the mean altitude of the model sigma level. Rayleigh friction is applied only near the surface ($\sigma > 0.8$). Sixth-order horizontal diffusion is used throughout the domain. The model equations and definitions of the vertical levels can be found in the appendix of *Song and Robinson* [2004].

[6] For each ensemble member, the seasonal transition begins from a different day of a long winter equilibrium run of the model run. The stratospheric radiative equilibrium temperature, T_{eq}, then performs a 180-day sinusoidal transition from winter to summer, given by:

$$T_{eq} = T_{eq\_\mathbf{winter}} + \sin^2(\pi t/360\,\mathrm{day}) \times \left(T_{eq\_\mathbf{summer}} - T_{eq\_\mathbf{winter}}\right) \qquad (2)$$

[7] We follow BMR to construct composites of the final warmings. Each final warming event is identified as the final time at which the zonal mean zonal wind at 50 hPa and 70° latitude becomes easterly and never again exceeds a threshold westerly strength (BMR). Composite final warmings are constructed by performing ensemble averages with the time of each member shifted in time so that their onset times are aligned. The "climatological" ensemble average is constructed in a similar way, but now shifting each member in time so that the temporal evolutions of T_{eq} are the aligned. Composite anomaly fields are formed by subtracting the ensemble climatology from the ensemble composite.

[8] Two types of final warmings are simulated: with and without topography. These roughly represent Earth's Northern and Southern Hemispheres. For the topography simulations, the Rockies and Himalayas are represented by one 3000 m and one 5000 m mountain, centered at 45° latitude and separated by 180 degrees of longitude. For the topography runs the radiative equilibrium stratospheric jet is set to 120 m/s, and for the non-topography runs it is set to 150 m/s.

[9] For the no-topography runs, both hemispheres make the spring transition simultaneously, whereas for the topography runs, the transition occurs only in the "Northern" Hemisphere – the hemisphere with topography - while the other hemisphere experiences the opposite fall transition (otherwise the two hemispheres interact via their topographic stationary waves). Each ensemble has 40 members, so, assuming that the hemispheres behave independently in the no-topography model, there are 40 independent final warmings with topography and 80 without topography.

3. Results

[10] As in nature, the stratospheric final warmings in the GCM occur at a range of times relative to the radiatively imposed spring transition. Figure 1 shows histograms of the onset date for the non-topography and topography final warmings. In the no-topography model the final warming dates vary over more than 100 days, but with a well-defined peak in the distribution. In the topography model, the range of warming dates is similar, but the distribution is nearly flat. If we consider the starting date of the radiative transition to be the winter solstice set (approximately Dec 21 or June 21), the mean warming date for the no-topography model (day +162) corresponds to Nov 30, which is in reasonable agreement with the observed average warming date in the Southern Hemisphere, Dec 4 [*Black and McDaniel*, 2007a]. The mean

[1] Auxiliary materials are available in the HTML. doi:10.1029/2008GL036624.

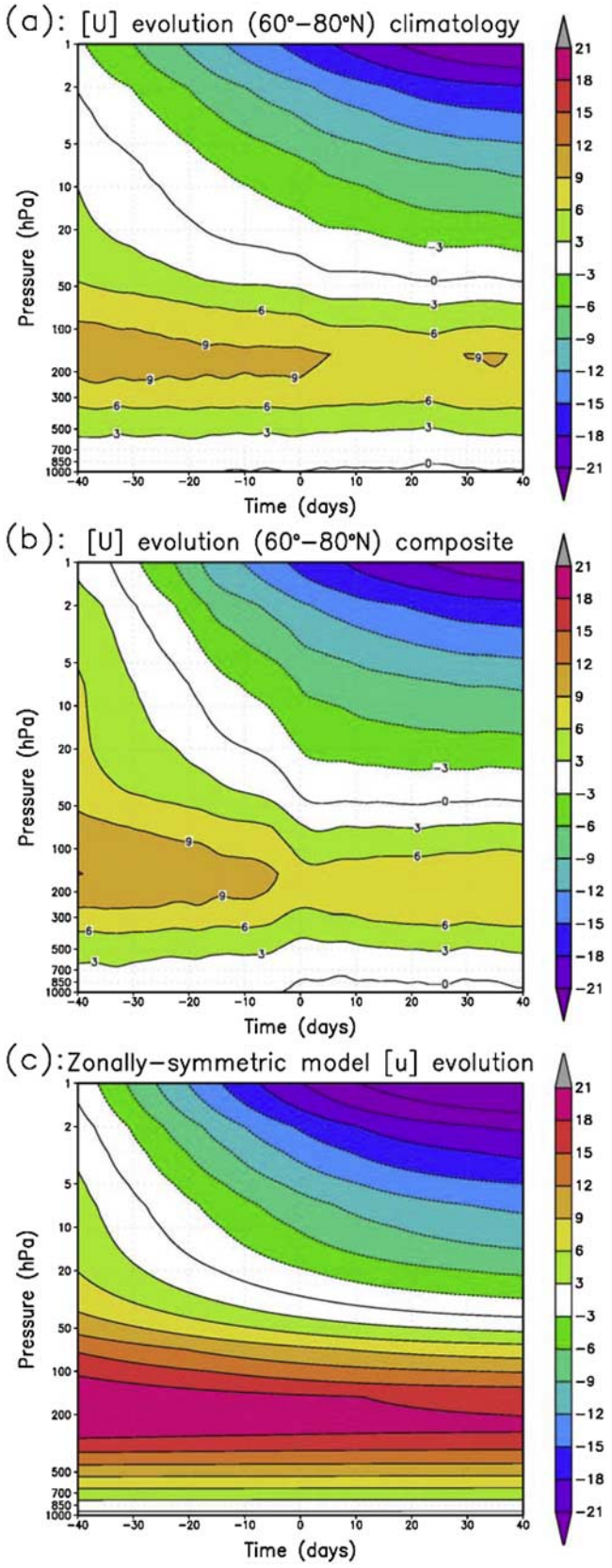

onset time for the topography cases (day +152), however, is much later than the observed average final warming date of April 14 (corresponding to day 114) in the Northern Hemisphere (BMR). This discrepancy may be explained by the fact that our simulated winter state with topography has a stratospheric jet that is much stronger than is observed in boreal mid-winter. Together with the absence of stratospheric sudden warming in the model's spring transition, it indicates that the role of planetary waves in the stratosphere for the topographic final warming simulation is less than in the NH observations. The standard deviations of the final warming onset time in our simulation are 18 days for the non-topography and 26 days for the topography cases, larger but similar to the 13 days for the austral observation [*Black and McDaniel*, 2007a] and 18 days in the NH (BMR gave only the standard deviation for 10 hPa onset times; we expect the values will be slightly larger for 50 hPa onset times).

[11] The climatology and composite high-latitude (60°–80° Lat) zonal mean zonal wind evolutions for the topography final warmings are compared in Figures 2a and 2b. (The composite and climatology zonal winds for the non-topography final warmings are similar.) The climatology is characterized by a transition from wintertime westerlies to summertime easterlies in the stratosphere. In the troposphere, a perceptible deceleration of zonal wind occurs; near the surface the zonal winds change sign after the final warming onset. The zonal wind transition of the composite is more abrupt than in the climatology in both the stratosphere and the troposphere. We also simulate the final warming in a zonally symmetric version of the GCM model: shown in Figure 2c. While the zonal wind transition in the stratosphere resembles the full-model climatology, the zonal winds in the troposphere are much stronger, due to the absence of eddies, and are unaffected by the final warming.

[12] As explained in the methods section, we composite the zonal wind anomalies with respect to the final warmings. The composite high-latitude (60°–70° Lat) zonal mean zonal winds for the non-topographic and topographic final warmings are shown in Figures 3a and 3b. For both types of events, westerly anomalies appear prior to the stratospheric final warming, extending from the stratosphere to the surface, with easterly anomalies appearing afterwards. For the non-topography events, the easterly anomalies after the warming occur in three stages: near day +2 when the stratospheric anomalies peak, they extend downward into the troposphere briefly; one week later, after the stratospheric anomalies have weakened, the tropospheric anomalies become stronger; after day 20, when the stratospheric anomalies have nearly vanished, perceptible easterly anomalies persist in the troposphere. The pattern is similar for the topography final warmings (Figure 3b) but the anomalies are stronger, and their extension down into the troposphere is similar to what BMR found in observations. Moreover,

Figure 2. The daily time evolution of zonal-mean zonal wind averaged from 60° to 80° latitude. (a) Climatological-mean time evolution for the topography final warming events. (b) Parallel time evolution for the composite constructed with respect to the timing of 50 hPa topography final warming events. (c) Same as in Figure 2a but for the zonally symmetric model. The contour interval is 3 m/s.

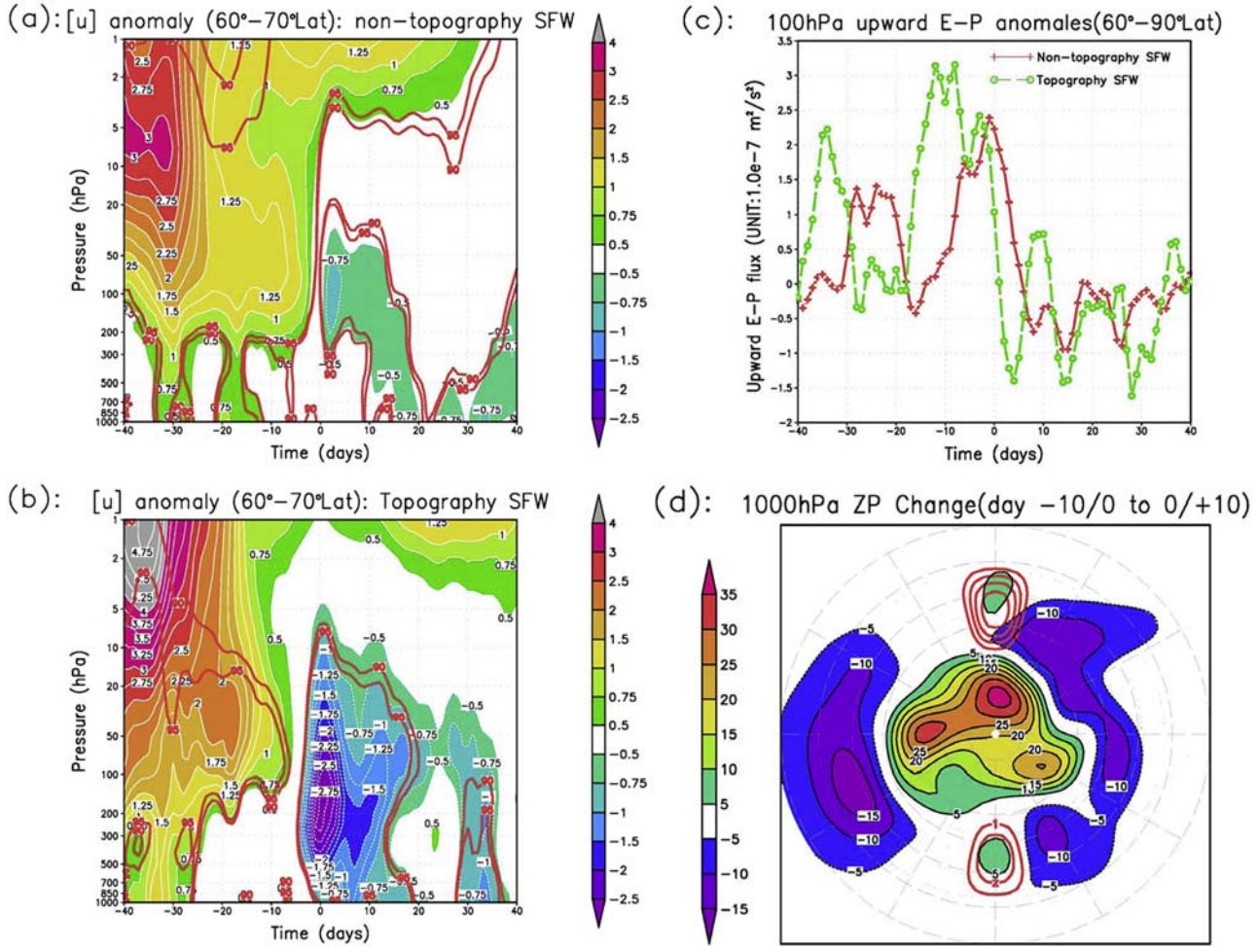

Figure 3. (a) Composite 60°–70° latitude averaged zonal-mean zonal wind anomalies with respect to the timing of the non-topography final warming events. Red lines indicate 90% and 95% confidence level for a 2-side student t-test. The anomaly contour interval is 0.25 m/s. (b) Same as in Figure 3a, but for the topography final warming events, and the contour interval is 0.5 m/s. (c) Composite high latitude upward EP flux anomalies at 100 hPa with respect to the timing of the topographic and non-topographic final warming events. The units are 1.0×10^{-7} m^2/s^2. (d) Shaded contours show the change in 1000 hPa geopotential height anomalies across the topography final warming events. The contour interval is 5 m. The red contours show the height of the topography. The interval is 1 km.

the simulated differences between non-topography and topography events are consistent with observed differences between final warmings in the Northern and Southern Hemispheres.

[13] Previous studies showed that anomalously strong upward Eliassen-Palm (EP) fluxes near the tropopause precede disturbances of the stratospheric circulation, most notably mid-winter sudden warmings [*Scott and Polvani*, 2004; *Polvani and Waugh*, 2004]. In our simulations, the deceleration of the stratospheric zonal wind leading to the final warming is similarly associated with upward EP flux anomalies and EP convergence. Figure 3c shows the composite high-latitude upward EP flux anomalies at 100 hPa for both types of final warmings. Between day −5 and day 0, stratospheric zonal winds decelerate in association with anomalously strong upward EP fluxes. Earlier, there are precursor amplifications of the EP flux; these occur at day −25 for the non-topographic warmings and at day −35 for the topographic warmings. Most of this wave flux is due to wave numbers 1–3.

[14] Changes in the tropospheric circulation across the final warmings are revealed by the changes in the 1000 hPa geopotential height anomalies shown in Figure 3d, for the topography final warmings. Plotted is the change in the anomalous geopotential height associated with the final warming, computed by subtracting the height anomaly averaged over the 10 days preceding the final warming from the height anomaly averaged over the 10 days following the event. During the breakdown of the polar vortex, tropospheric geopotentials increase in the Polar Regions and decrease in surrounding latitudes. This pattern projects onto the negative phase of the familiar Arctic Oscillation [*Thompson and Wallace*, 1998], but includes significant zonal asymmetries, with the region of greatest increases displaced well off the pole. In contrast, the climatological changes in geopotential heights across the final warming (not shown) have increasing heights across most of the extratropics. Despite the use of idealized topography these geopotential height changes are similar in pattern and magnitude to those that occur across

observed Northern Hemisphere final warmings (see Figure 4 of BMR).

[15] Five-member ensembles with increased horizontal (rhomboidal 60 spherical-harmonic truncation, R60L30) and vertical resolution (60 vertical levels, R30L60) have been performed to test the sensitivity of the model to resolution. While these changes in resolution affect the wintertime internal variability of the model, the results for the final warming are largely unaffected.

4. Summary

[16] A modeling study has been carried out to investigate the downward influence of stratospheric final warming events in models with and without topography. We find that zonally symmetric dynamics, as represented in a zonally symmetric version of our model, do not produce a downward influence of final warmings on the tropospheric circulation. In our full models however, final warmings occur with realistically variable timing and they significantly affect the troposphere. Because, in our model, the seasonal transition is imposed only in the stratosphere, these results suggest that a substantial fraction of the observed tropospheric changes that occur in conjunction with the final warming are induced from the stratosphere. This further suggests that the role of the stratosphere in the climate, and, more practically, the value of including a well-resolved stratosphere in climate models, should be considered in the context of the full seasonal cycle. In addition, pulses of upward wave-activity flux precede the final warmings in our model, as in observations, although the time of these pulses differs between our model and the atmosphere. This gives us increased confidence that the precursors in the observations are real and reproducible features of the spring transition.

[17] Overall, these results lends support to the idea that the stratosphere plays an important dynamical role in the springtime transition in the lower atmosphere, and thereby motivate continued efforts to understand the dynamics of EP-flux precursors to the final warming and their subsequent downward influence.

[18] **Acknowledgments.** This study is supported by the NSF Climate and Large-scale Dynamical Program under grant ATMS-0456157. It is based upon work carried out by while WR served at the National Science Foundation. Any opinion, findings, and conclusions or recommendations expressed in this material are those of the authors and do not necessarily reflect the views of the NSF.

References

Andrews, D. G., J. R. Holton, and C. B. Leovy (1987), *Middle Atmospheric Dynamics*, 489 pp., Academic, Orlando, Fla.

Black, R. X., and B. A. McDaniel (2007a), Interannual variability in the Southern Hemisphere circulation organized by stratospheric final warming events, *J. Atmos. Sci.*, *64*, 2968–2974.

Black, R. X., and B. A. McDaniel (2007b), The dynamics of Northern Hemisphere stratospheric final warming events, *J. Atmos. Sci.*, *64*, 2932–2946.

Black, R. X., B. A. McDaniel, and W. A. Robinson (2006), Stratosphere-troposphere coupling during spring onset, *J. Clim.*, *19*, 4891–4901.

Held, I. M., and M. J. Suarez (1994), A proposal for the inter-comparison of the dynamical cores of atmospheric general circulation models, *Bull. Am. Meteorol. Soc.*, *75*, 1825–1830.

Holton, J., and C. Mass (1976), Stratospheric vacillation cycles, *J. Atmos. Sci.*, *33*, 2218–2224.

Kushner, P. J., and L. M. Polvani (2004), Stratosphere-troposphere coupling in a relatively simple AGCM: The role of eddies, *J. Clim.*, *17*, 629–639.

Polvani, L. M., and P. J. Kushner (2002), Tropospheric response to stratospheric perturbations in a relatively simple general circulation model, *Geophys. Res. Lett.*, *29*(7), 1114, doi:10.1029/2001GL014284.

Polvani, L. M., and D. W. Waugh (2004), Upward wave activity flux as a precursor to extreme stratospheric events and subsequent anomalous surface weather regimes, *J. Atmos. Sci.*, *17*, 3548–3554.

Reichler, T., P. J. Kushner, and L. M. Polvani (2005), The coupled stratosphere–troposphere response to impulsive forcing from the troposphere, *J. Atmos. Sci.*, *62*, 3337–3352.

Scinocca, J. E., and P. H. Haynes (1998), Dynamical forcing of stratospheric planetary waves by tropospheric baroclinic eddies, *J. Atmos. Sci.*, *55*, 2361–2391.

Scott, R. K., and L. M. Polvani (2004), Stratospheric control of upward wave flux near the tropopause, *Geophys. Res. Lett.*, *31*, L02115, doi:10.1029/2003GL017965.

Song, Y., and W. A. Robinson (2004), Dynamical mechanisms for stratospheric influences on the troposphere, *J. Atmos. Sci.*, *61*, 1711–1725.

Thompson, D. W. J., and J. M. Wallace (1998), The Arctic Oscillation signature in the wintertime geopotential height and temperature fields, *Geophys. Res. Lett.*, *25*, 1297–1300.

W. A. Robinson, Division of Atmospheric Sciences, National Science Foundation, 4201 Wilson Boulevard, Arlington, VA 22230, USA.

L. Sun, Department of Atmospheric Sciences, University of Illinois at Urbana-Champaign, 105 South Gregory Street, Urbana, IL 61801, USA. (lsun3@atmos.uiuc.edu)